

# Scanning tunneling spectroscopy of a-axis $\text{YBa}_2\text{Cu}_3\text{O}_{7-\delta}$ films: $k$ -selectivity and the shape of the superconductor gap

A. SHARONI<sup>1</sup>, G. LEIBOVITCH<sup>2</sup>, A. KOHEN<sup>2</sup>, R. BECK<sup>2</sup>, G. DEUTSCHER<sup>2</sup>,  
G. KOREN<sup>3</sup> and O. MILLO(\*)<sup>1</sup>

<sup>1</sup> *Racah Institute of Physics, The Hebrew University, Jerusalem 91904, Israel*

<sup>2</sup> *School of Physics and Astronomy, Raymond and Beverly Sackler Faculty of Exact Science, Tel Aviv University, 69978 Tel Aviv, Israel*

<sup>3</sup> *Department of Physics, Technion - Israel Institute of Technology, Haifa 32000, Israel*

PACS. 74.50.+r – Proximity effects, weak links, tunneling phenomena, and Josephson effects.

PACS. 74.72.Bk – Y-based cuprates.

PACS. 74.80.-g – Spatially inhomogeneous structures.

**Abstract.** – Tunneling spectroscopy of epitaxial (100) oriented  $\text{YBa}_2\text{Cu}_3\text{O}_{7-\delta}$  films was performed using an STM at 4.2 K. On atomically smooth areas, tunneling spectra revealing clear U-shaped gaps with relatively low zero bias conductance were measured. These spectra can be well fitted to the tunneling theory into a d-wave superconductor only when introducing a strong dependence of the tunneling probability on the wave-vector  $k$ . Possible origins for this  $k$ -selectivity in STM measurements will be discussed. On other areas, V-shaped gaps as well as zero bias conductance peaks are observed, indicating relaxation of  $k$ -selectivity and the effect of nanofaceting, respectively.

The  $d$ -wave symmetry of the order parameter of  $\text{YBa}_2\text{Cu}_3\text{O}_{7-\delta}$  (YBCO) [1, 2, 3] has a special signature in the tunneling spectra measured for these superconductors. The hallmark of this is the zero bias conductance peak (ZBCP) that appears when tunneling along or near the nodal direction ([110] for YBCO). This reflects the existence of Andreev bound states at the Fermi level residing on the pair-breaking (110) surface [4, 5, 6, 7, 8]. The ZBCP was measured by numerous groups, using both macroscopic and microscopic (STM) tunnel junctions [9, 10, 11, 12, 13, 14, 15]. Manifestation of the  $d$ -wave order parameter in the tunneling spectra acquired along the anti-nodal ([100] for YBCO) and the  $c$ -axis directions is more controversial. The theory of tunneling into a  $d$ -wave superconductor predicts a V-shaped gap structure for both tunneling directions in the case where the density of states (DOS) is isotropically averaged over the Fermi surface [6, 7]. Here, quasi-particle excitations are observed at any finite energy, since the nodal directions in  $k$ -space are monitored, resulting in a linear dependence of the  $dI/dV$  vs.  $V$  tunneling spectra on energy around the Fermi energy (zero bias). Such isotropic tunneling scenario is believed to apply to STM measurements [16]. In contrast, U-shaped gaps are predicted to appear when  $k$ -vectors along the anti-nodal direction are preferentially monitored in the tunneling process [7, 11, 14, 17, 18]. Resolving this issue is thus important for

---

(\*) Corresponding author, e-mail: milode@vms.huji.ac.il

understanding STM spectroscopy in high temperature superconductors and other anisotropic systems.

Experimentally, V-shaped gaps are indeed commonly observed in c-axis tunneling measurements [7, 11, 14, 19, 20, 21, 22]. Recently, however, U-shaped gaps were observed in tunneling spectra acquired on the (001)  $\text{Bi}_2\text{Sr}_2\text{CaCu}_2\text{O}_{8+\delta}$  (BSCCO) surface [17]. This was accounted for by a ‘ $k$ -selection mechanism’ inducing preferential tunneling along the anti-nodal directions, resulting from the large overlap, and consequently strong coupling, between the tip’s electronic states and the  $3d$  orbitals of the Cu atoms, through the mediation of their  $4s$  states [23]. However, a corresponding effect was not yet established for the  $a$ -axis surface, where direct coupling to the Cu atoms is possible.

The data reported for  $a$ -axis tunneling is much more diverse, possibly due to problems in preparing well-defined (100) cuprate surfaces, and keeping the exposed Cu-O planes from deterioration. A wide range of features were observed, including zero bias peak structures, mostly inside gaps [11, 13, 24], as well as V-shaped [25, 26] and U-shaped gaps [18, 27]. The zero bias conductance peak may result from nano-faceting or roughness of the measured surface, as has been demonstrated by various groups [14, 21, 28, 29]. The U-shaped gaps were accounted for by assuming a narrow tunneling cone centered along the anti-nodal direction, although, as will be shown below, the ‘orbital coupling’ model discussed above may apply as well.

In this paper we present an extensive scanning tunneling spectroscopy study of (100) YBCO surfaces, directed at resolving some of the questions arising from the contradictory experimental findings described above. We have measured films prepared using two different deposition techniques, DC sputtering and laser ablation. For both film types, spectra exhibiting U-shaped gaps with relatively low zero bias conductance are found on smooth areas. These spectra are well fitted to the tunneling theory into a  $d$ -wave superconductor only when introducing a tunneling probability that is preferentially strong along the anti-nodal directions. However, we cannot distinguish between the ‘orbital coupling’ and the ‘tunneling cone’ models. In areas showing a rougher topography, only V-shaped gaps and zero bias conductance peaks (ZBCP) of varying strength are observed.

Epitaxial thin YBCO films of various types were prepared by either DC sputtering or laser ablation, with relatively broad transitions, onset at 86 (88) K and ending at 82 (81) K for the DC-sputtered (laser ablated) films. Both preparation methods produced films yielding very similar spectroscopic data in spite of the different morphology.  $\text{YBa}_2\text{Cu}_3\text{O}_{7-\delta}$  with 5% Ca doping were grown on  $\text{LaAlO}_3$  substrates by DC off-axis sputtering, applying the method described in Ref. [30] for c-axis films. Here, however, the deposition temperature was reduced to  $720^\circ\text{C}$  in order to promote the development of  $a$ -axis crystallite outgrowths [31]. These films consisted of dense arrays of rectangular  $a$ -axis crystallites, typically 20 nm in height and a few hundreds of nm in size, covering 70-90% of the surface area, as confirmed by X-ray diffraction, Atomic Force Microscopy (AFM) and Scanning Electron Microscopy (SEM). Many of these crystallites had large atomically smooth areas on the top. The STM and AFM images in Figs. 1a and 1b exhibit the surface morphology of these films, showing a single crystal (and a junction with its neighbor) and an array structure, respectively. We have also measured DC sputtered  $a$ -axis YBCO films prepared using the procedure described in Ref. [24], also showing large flat areas.

The laser-ablated films were grown on (100)  $\text{SrTiO}_3$  wafers by two different dual-step processes. First, a 30 nm thick YBCO layer was prepared at a wafer temperature of  $600^\circ\text{C}$  (or  $650^\circ\text{C}$ ). Then, a second 75 nm thick YBCO layer was deposited at  $750^\circ\text{C}$  (or  $785^\circ\text{C}$ ). The films prepared at the higher temperatures displayed  $a$ -axis crystallite outgrowths on a c-axis background, similar to the DC sputtered films, as depicted in the STM image of Fig. 1c. The lower deposition temperature produced films with two coexisting  $a$ -axis phases on

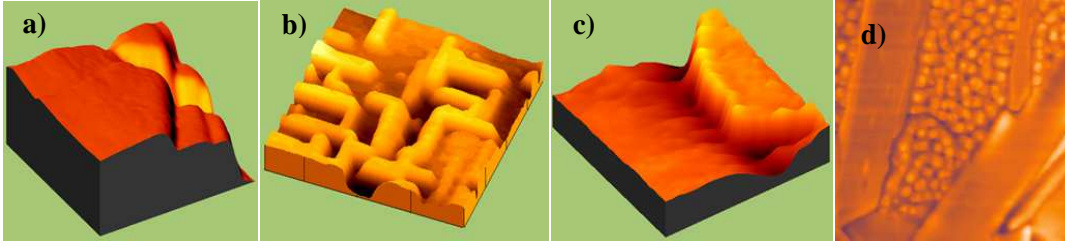


Fig. 1 – STM and AFM images portraying the surface morphology of YBCO films containing various degrees of c-axis (background) and a-axis (outgrowth) orientations. (a) and (b) - DC sputtered YBCO films with about 70% a-axis orientation, where (a) is a  $180 \times 180 \text{ nm}^2$  STM topographic image focusing on a single a-axis crystallite, 25 nm in height, and (b) is a  $1.6 \times 1.6 \mu\text{m}^2$  AFM image showing an array of outgrowing crystallites, having atomically smooth areas on the scale of a few tens of nm. (c) and (d) - laser ablated films, where (c) is a  $35 \times 35 \text{ nm}^2$  STM image displaying a single outgrowing a-axis crystallite, 20 nm in height, and (d) is a  $2 \times 2 \mu\text{m}^2$  AFM image of a 95% a-axis film exhibiting two types of areas. The first is composed of small crystallites a few unit cells in height, while the second consists of large areas, atomically smooth on scales of 100 nm.

about 95% of the film area (as determined by X-ray diffraction). One phase consisted of small crystallites, a few unit-cells in height, while the other is composed of large areas, atomically smooth on scales of hundreds of nanometers, as depicted by the AFM image in Fig. 1d.

The samples were transferred directly from the growth chamber into a chamber that was over-pressured by dry oxygen, then mounted within a few hours into a home made cryogenic STM and cooled down to 4.2 K in He exchange gas, being exposed to air for less than 15 minutes. A total of 5 sputtered films and 4 laser-ablated films were measured. The tunneling  $dI/dV$  *vs.*  $V$  curves were acquired either directly by the use of conventional lock-in technique, or by numerical differentiation of the measured  $I$ - $V$  curves, with similar results obtained by both methods. We have confirmed that the measured gaps and ZBCP features were independent of the STM voltage and current setting (before disconnecting momentarily the feedback circuit). This rules out the possibility that the gap features are due to the Coulomb blockade, which is known to be sensitive to these parameters [32]. All the STM data presented in this paper were acquired at 4.2 K with (normal) tunneling resistances between 100 M $\Omega$  to 1 G $\Omega$ .

On all the measured samples we have found atomically smooth areas, on the scale of tens of nanometers or more, where the  $dI/dV$  *vs.*  $V$  curves featured mainly U-shaped gaps, with relatively low zero bias conductance. The gap value distribution in these regions was relatively narrow, varying between 16 to 18 meV, for both laser ablated and DC sputtered films. Typical measurements are presented in fig. 2 (empty circles), where spectrum 2a was measured on the laser-ablated film, on the a-axis crystallite shown in fig. 1c, and spectrum 2b is a representative example for the sputtered films, acquired on the crystallite shown in image 1a. The inset of fig. 2a presents the  $I(V)$  curve from which the differential conductance was derived, depicting a BCS-like structure. The red curves were calculated using the theory for tunneling into  $d$ -wave superconductors [6, 7], taking an equal weight for all  $\mathbf{k}$ -vectors, i.e., an isotropic tunneling matrix. It is clear that the V-shaped gap structure thus obtained deviates considerably from the experimental curves at the low energy regime, the experimental curves being by far more flat. The blue curves in fig. 2, on the other hand, were calculated assuming preferential tunneling in the anti-nodal directions. In fig. 2a we used the ‘orbital

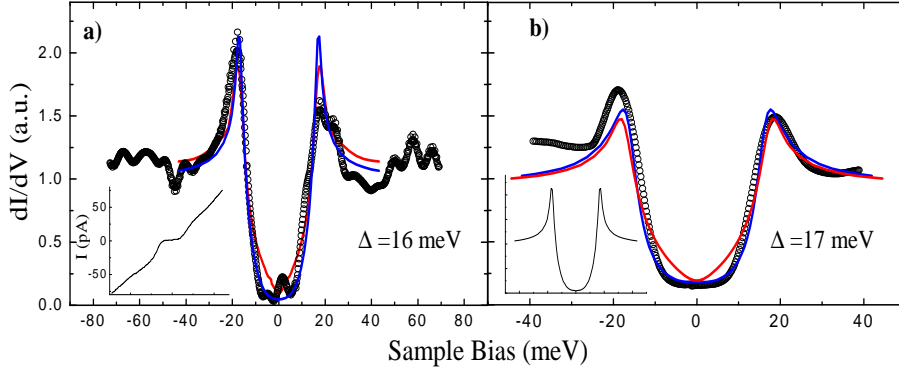


Fig. 2 – a) A tunneling spectrum measured on the a-axis crystallite shown fig. 1c (empty circles), with the corresponding I-V curve shown in the inset. The blue curve is a fit using the ‘orbital coupling’ model with a 16 meV gap and  $\Gamma = 0.06\Delta$ . b) A spectrum measured on the crystallite shown in fig. 1a (empty circles), fitted to the ‘narrow tunneling cone’ model,  $\Delta = 17$  meV and  $\Gamma = 0.1\Delta$ . An equally good fit was obtained for the ‘orbital coupling’ model, shown in the inset. For comparison, we present spectra calculated assuming isotropic averaging over the Fermi surface, with the same  $\Delta$  and  $\Gamma$  values, showing a large deviation from the measured spectra at the low bias region (red curves).

coupling’ model, whereas in fig. 2b the ‘narrow tunneling cone’ approach was applied, both reproducing well the measured U-shaped gap structure.

For the ‘orbital coupling’ model we used the tunneling matrix element given by Misra et al. [17],  $|M(k)|^2 \propto [\cos(k_x a) - \cos(k_y a)]$ , where  $k_x$  and  $k_y$  are the wave vector components along the main axes in the a-b plane. Note that this model was applied in Ref. [17] to c-axis tunneling. However, it should also be valid for tunneling into the (100) surface, where the lobe of the Cu *d*-orbital is perpendicular to the surface, thus strongly overlapping directly with the tip states. The blue curve in fig. 2a was calculated using this model, with a gap of  $\Delta = 16$  meV and a small Dynes broadening parameter [33],  $\Gamma = 0.06\Delta$ , showing good agreement with the experimental data in the gap region. Equally good fits were obtained using the ‘narrow tunneling cone’, described below.

The ‘narrow tunneling cone’ model is, in a sense, a semi-classical approach. Within the WKB approximation, and at bias voltages much smaller than the tunneling barrier height  $\Phi$ , the tunneling transition probability decays exponentially with increasing  $k_T$ , the transverse component of the wave vector  $\mathbf{k}$ :  $p(\mathbf{k}) \propto \exp[-\{\hbar^2 d / (2m\Phi)^{1/2}\} k_T^2]$ , and consequently  $p(\theta) \propto \exp[-\beta \sin^2(\theta)]$ . Here,  $\theta$  is the angle between the momentum of the tunneling electron and the surface normal and  $\beta = \sqrt{2m/\hbar^2} \frac{E_F}{\sqrt{\Phi}} d$ , where  $E_F$  is the Fermi energy and  $d$  is the width of the tunneling barrier [11, 18, 34, 35]. For typical tunneling junctions, this will result in a narrow tunneling-momentum cone around the surface normal ( $\Delta\theta \sim 20^\circ$ , full angle).

This type of reasoning doesn’t alter the characteristics of tunneling in the [110] or the [001] direction, but predicts a U-shaped gap for the (100) surface. Figure 2b demonstrates a fit obtained using this model with  $\Delta = 17$  meV and  $\Gamma = 0.1\Delta$ . This particular fit was calculated with  $\Delta\theta = 20^\circ$ , but no significant difference is found in the range of  $0^\circ < \Delta\theta < 30^\circ$ . In the inset we present, for comparison, a nearly identical spectrum calculated using the ‘orbital coupling’ model. We were not able, in this work, to differentiate between these two models, but it is clear that a  $\mathbf{k}$ -selection mechanism is essential to account for our results.

It should be pointed out that V-shaped curves obtained from the isotropic tunneling model,

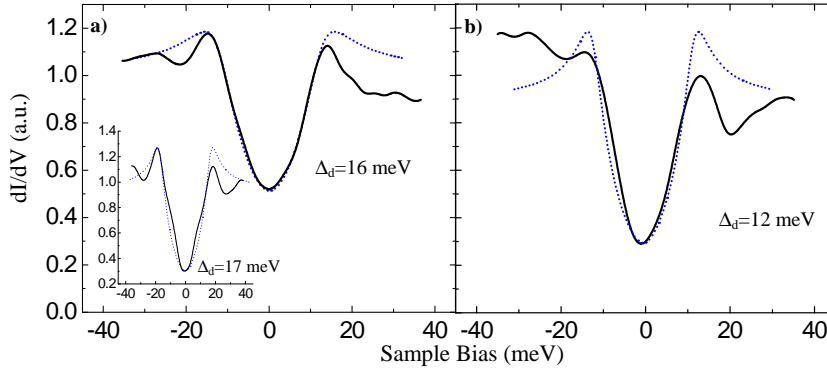


Fig. 3 – Tunneling spectra displaying V-shaped gaps. a) Spectrum measured on a rough region of the laser ablated sample shown in fig. 1d. Inset: Spectrum measured on an a-axis outgrowth. b) Spectrum taken on a sputtered film. In both a) and b), the dotted curves are fits calculated assuming an isotropic tunneling probability, with gap values indicated in the figure and  $\Gamma = 0.1\Delta$  for the inset and about  $0.2\Delta$  for the other two curves.

such as those presented in red in fig. 2, can be smeared using very large Dynes broadening parameter until a structure resembling U-shaped gaps would emerge. Then, however, the zero bias conductance becomes much larger than that of the experimental data.

In areas having a larger degree of surface roughness and disorder, U-shaped gaps were never observed, and the spectra showed only V-shaped gaps or ZBCPs. The zero bias conductance in these curves were typically larger as compared to the U-shaped spectra, varying between 20% to 50% of the normal differential conductance (at high bias). Best fits of these data are obtained using the isotropic tunneling-probability model with a lifetime broadening of around  $0.2\Delta$ . Fits with any of the  $\mathbf{k}$ -selective models described above, yield unreasonably large Dynes parameters of more than  $0.5\Delta$ . In fig. 3 we present typical V-shaped gap structures measured on various film types, along with the corresponding fits depicted by the dotted curves, with gap values denoted in the figure. The spectra in fig. 3a were measured on the two types of laser-ablated films. The one in the mainframe was taken on a rough part of the film shown in fig. 1d, and the other in the inset is for an a-axis crystallite outgrowth, both showing a fairly low zero bias conductance. The data in 3b was acquired on an a-outgrowth from a DC sputtered film. The relatively small gap in this figure may be due to local deviations from optimal doping resulting from losses of oxygen from the surface. The gap distribution in these regions were much larger as compared to the smooth ones, varying between 12 to 17 meV, with no apparent dependence on film preparation method.

As mentioned earlier, the U-shaped gaps were found only on smooth areas, whereas V-shaped structures are typically measured on more disordered regions. A question then arises regarding the role played by the local surface morphology on the measured spectra. Since the typical gap size for both gap shapes (and also in the presence of a ZBCP, see below) is the same, around 17 meV, it appears that the local surface roughness does not affect much the order parameter at the surface. We note in passing that our data are in agreement with Ref. [36], where similar gap values were obtained for both [110] and [100] orientations, further confirming the conclusion [36] that YBCO is in the  $d$ -wave weak coupling regime. However, surface disorder is known to relax conservation rules for the in-plane component of the  $\mathbf{k}$ -vector, and in our case, may wash out the strong  $\mathbf{k}$ -dependent tunneling probabilities introduced in either the ‘orbital coupling’ or ‘narrow tunneling cone’ models. Surface roughness seems also to affect

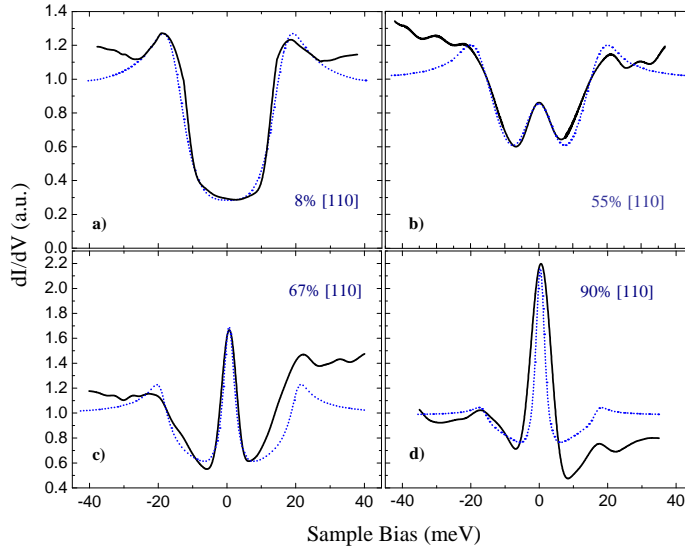


Fig. 4 –  $dI/dV$  *vs.*  $V$  curves measured on a faceted region on the YBCO film shown in fig. 1d. The curves can be fitted well by a ‘two channel’ tunneling model, assuming independent contributions of tunneling in the [110] and [100] directions. The same  $\Delta = 17$  mV and  $\Gamma = 0.15\Delta$  were used in all 4 panels, and the different relative contribution of [110] tunneling is indicated in each panel. The fits presented here were calculated with the ‘narrow tunneling cone’ model, but similar fits are achieved with the ‘orbital coupling’ model.

the quasi-particle life-time at the surface, smearing the gap structure and thus enhancing the Dynes parameters needed for the fits.

Another typical spectral feature that we have found is a ZBCP embedded in a gap structure, resembling  $dI/dV$ - $V$  characteristics obtained for macroscopic tunnel junctions on (100) YBCO surfaces [13,24]. This behavior was attributed to the effect of (110) facets. Indeed, STM measurements have shown that even a facet of unit-cell height can give rise to a ZBCP [14,28]. Such a local sensitivity was not yet demonstrated for the (100) YBCO surface. In fig. 4 we present spectra exhibiting ‘peak in a gap’ structures measured on a faceted (rough) region of the laser ablated film shown in fig. 1d, where the relative ZBCP height increases from 4a (no visible peak) to 4d. The curves can be fit well by employing a ‘two channel’ model, where independent contributions of tunneling in the [110] and [100] directions are taken into account. The magnitude of the [110] tunneling component varies spatially, as is indicated in each figure, whereas the gap and the Dynes parameters were nearly the same,  $\sim 17$  meV and  $0.15\Delta$ , respectively. The fit to the U-shaped gap in fig. 4a requires a  $\mathbf{k}$ -selective tunneling process. However, due to the relatively large zero bias conductance level (as compared to other U-shaped gaps), a small [110] contribution had to be included; (the peak structure is washed out due the broadening parameter).

In conclusion, our data provide clear evidence that the local tunneling spectra acquired for a-axis YBCO films do not always reflect the bulk superconductor DOS averaged isotropically over the Fermi surface. Tunneling characteristics exhibiting U-shaped gap structures, rather than the V-shapes, are often measured. The observation of U-shaped gaps does not depend on the sample preparation method, but is correlated with the degree of surface smoothness.

Two possible models that reproduce equally well these spectra were considered: a narrow tunneling cone around the [100] normal direction, and a strong overlap of the tip electronic states with the *d*-wave electronic orbitals of the Cu ions emerging out of the surface, both enhance tunneling preferentially along the anti-nodal directions.

\* \* \*

This work was supported in parts by the Israel Science Foundation, the Heinrich Hertz-Minerva Center for High Temperature Superconductivity, and by the Oren Family Chair for Experimental Solid State Physics.

## REFERENCES

- [1] ORENSTEIN J. and MILLIS A. J., *Science*, **288** (2000) 468.
- [2] VAN HARLINGEN D. J., *Rev. Mod. Phys.*, **67** (1995) 515.
- [3] TSUEI C. C. and KIRTLEY J. R., *Rev. Mod. Phys.*, **72** (2000) 969.
- [4] BRUDER C., *Phys. Rev. B*, **41** (1990) 4017.
- [5] HU, C. R., *Phys. Rev. Lett.*, **72** (1994) 1526.
- [6] TANAKA Y. and KASHIWAYA S., *Phys. Rev. Lett.*, **74** (1995) 3451.
- [7] KASHIWAYA S., TANAKA Y., KOYANAGI M. and KAJIMURA K., *Phys. Rev. B*, **53** (1996) 2667.
- [8] BARASH YU. S., SVIDZINSKY A. A. and BURKHARDT H., *Phys. Rev. B*, **55** (1997) 15282.
- [9] COVINGTON M. *et al.*, *Phys. Rev. B*, **79** (1997) 277.
- [10] ALFF L. *et al.*, *Phys. Rev. B*, **55** (1997) R14757.
- [11] WEI J. Y. T., YEH N. C., GARRIGUS D. F. and STARSİK M., *Phys. Rev. Lett.*, **81** (1998) 2542.
- [12] DAGAN Y., KRUPKE R. and DEUTSCHER G., *Europhys. Lett.*, **51** (2000) 116.
- [13] IGUCHI I. *et al.*, *Phys. Rev. B*, **62** (2000) R6131.
- [14] SHARONI A., KOREN G. and MILLO, O., *Europhys. Lett.*, **54** (2001) 679.
- [15] SHARONI A. *et al.*, *Phys. Rev. B*, **65** (2002) 134526.
- [16] WIESENDANGER, R., *Scanning Probe Microscopy and Spectroscopy : Methods and Applications* (Cambridge University Press) 1995.
- [17] MISRA S. *et al.*, *Phys. Rev. Lett.*, **89** (2002) 87002.
- [18] SUZUKI K., ICHIMURA K., NOMURA K. and TAKEKAWA S., *Phys. Rev. Lett.*, **83** (1999) 616.
- [19] CHANG A. *et al.*, *Phys. Rev. B*, **46** (1995) 5692.
- [20] YEH N. C. *et al.*, *Physica C*, **364-365** (2001) 450.
- [21] UENO, S. *et al.*, *Physica C*, **357-360** (2001) 1576.
- [22] IAVARONE M. *et al.*, *Phys. Rev. B*, **65** (2002) 214506.
- [23] MARTIN I., BALATSKY A. V. and ZAAANEN J., *Phys. Rev. Lett.*, **88** (2002) 97003.
- [24] KRUPKE R. and DEUTSCHER G., *Phys. Rev. Lett.*, **83** (1999) 4634.
- [25] WANG W., YAMAZAKI M., LEE K. and IGUCHI I., *Phys. Rev. B*, **60** (1999) 4272.
- [26] KOREN G. and LEVY N. 59, 121 (2002)., *Europhys. Lett.*, **59** (2002) 121.
- [27] YEH, N.-C. *et al.*, *Phys. Rev. Lett.*, **87** (2001) 087003.
- [28] MISRA, S. *et al.*, *Phys. Rev. B*, **66** (2002) 100510R.
- [29] FOGELSTROM M., RAINER D. and SAULS J. A., *Phys. Rev. Lett.*, **79** (1997) 281.
- [30] KRUPKE R., BARKAY Z. and DEUTSCHER G., *Physica C*, **315** (1999) 99.
- [31] CHANG C. C. *et al.*, *Appl. Phys. Lett.*, **17** (1990) 1814.
- [32] BAR-SADEH E. and MILLO O., *Phys. Rev. B*, **53** (1996) 3482.
- [33] DYNES R. C., NARAYNAMURTI V. and GARNO J. P., *Phys. Rev. Lett.*, **41** (1978) 1509.
- [34] WOLF E. L., *Principles of Electron Tunneling Spectroscopy* (Oxford University press, Oxford) 1985.
- [35] WEI J. Y. T. *et al.*, *Phys. Rev. B*, **57** (1998) 3650.
- [36] DAGAN Y., KRUPKE R. and DEUTSCHER G., *Phys. Rev. B*, **62** (2000) 146.